Nanotechnology

ACCEPTED MANUSCRIPT

Vertically-aligned graphene nanowalls grown via plasma-enhanced chemical vapor deposition as a binder-free cathode in Li-O_2 batteries

To cite this article before publication: Chih-Pin Han *et al* 2018 *Nanotechnology* in press https://doi.org/10.1088/1361-6528/aae362

IOP Publishing Journal Title
Journal **XX** (XXXX) XXXXXX https://doi.org/XXXX/XXXX

Vertically-aligned Graphene Nanowalls Grown via Plasma-Enhanced Chemical Vapor Deposition as a Binder-free Cathode in Li-O_2 Batteries

Chih-Pin Han[1], Vediyappan Veeramani[1], Chen-Chih Hsu[2], Anirudha Jena[1,3], Ho Chang[3], Nai-Chang Yeh*[,2], Shu-Fen Hu*[,4], and Ru-Shi Liu*[1,3]

[1] Department of Chemistry, National Taiwan University, Taipei 106, Taiwan.
[2] Department of Physics, California Institute of Technology, Pasadena, California 91125, USA.
[3] Department of Mechanical Engineering and Graduate Institute of Manufacturing Technology, National Taipei University of Technology, Taipei 106, Taiwan.
[4] Department of Physics, National Taiwan Normal University, Taipei 116, Taiwan.

E-mail address: ncyeh@caltech.edu (Nai-Chang Yeh), sfhu.hu@ntnu.edu.tw (Shu-Fen Hu), rsliu@ntu.edu.tw (Ru-Shi Liu)

Received xxxxxx
Accepted for publication xxxxxx
Published xxxxxx

Abstract

In the present report, vertically-aligned graphene nanowalls are grown on Ni-foam (VA-G/NF) using plasma-enhanced chemical vapor deposition (PECVD) method at room temperature. Optimization of the growth conditions provides graphene sheets with controlled defect sites. The unique architecture of the vertically aligned graphene sheets allows sufficient space for the ionic movement within the sheets and hence enhancing the catalytic activity. Further modification with ruthenium nanoparticles (Ru NPs) drop-casted on VA-G/NF improves the charge overpotential for lithium-oxygen (Li-O_2) battery cycles. Such reduction we believe is due to the easier passage of ions between the perpendicularly standing graphene sheets thereby providing ionic channels

Keywords: Graphene nanowall, Ru Nanoparticles, Li-O_2 battery, Electrocatalyst.

1. Introduction

The technological revolution has dramatically raised the demand for energy, and intensive research has been carried out for efficient, cost-effective, and environment-friendly storage of energy [1-4]. Among all the class of batteries, the theoretical energy density of Lithium-oxygen (Li-O_2) batteries surpasses other lithium batteries [5, 6]. However, practically, Li-O_2 batteries only provide 0.5–1 KWh/kg energy density [7]. Nonetheless, for commercialization, several issues, such as low round-trip efficiency, large charging overpotential, and low practical energy density, need to be addressed. The working principle of the Li-O_2 battery is based on the following electrochemical reaction: $2Li^+ + 2e^- + O_2 \leftrightarrow Li_2O_2$ (E^o = 2.96 V). Li-O_2 batteries have three parts, namely, Li anode, an electrolyte, and a cathode. The Li_2O_2 product is formed at the interface of the cathode and electrolyte during discharge [8]. Moreover, the Li_2O_2 is insulating in bulk, however, half-metallic on the surface. Thus, decomposing during charging is difficult, resulting in the slow kinetics of oxygen reduction/evolution reaction (ORR/OER) [9]. Furthermore, low practical energy density affects battery performance. Abraham et al. discovered the first Li-O_2 battery in 1996 [10]. To date, carbon materials have been widely used by researchers because of their advantages, such as high electronic conductivity ($\sigma_{graphite} > 10^3$ S m^{-1}), low cost, and high specific surface area [6]. Therefore, many carbon materials have been developed in recent decades. High quality bottom graphene synthesis by PECVD at room temperature was founded by Boyd et al. [11]. Hsu et al. have used PECVD to grow graphene sheets with high aspect ratio on various

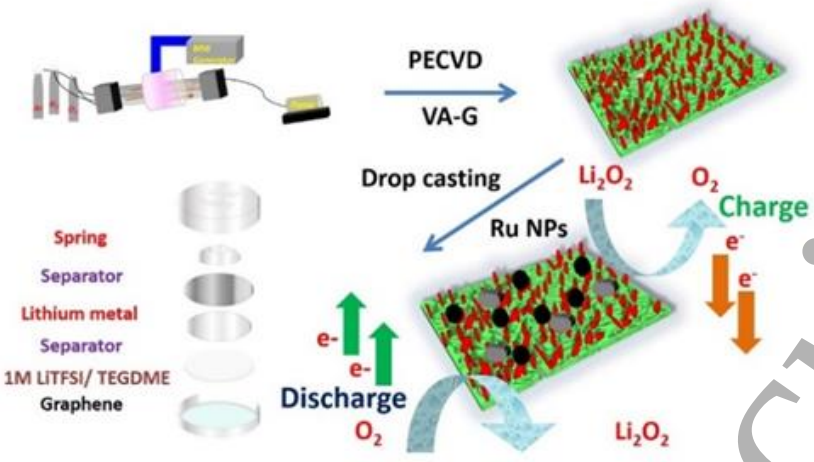

Scheme 1 Schematic illustration of the coin-cell fabrication process of Ru NPs/VA-G/NF materials as a cathode for the rechargeable Li-O_2 battery.

transition metal substrates [12]. Yang et al. have synthesized the mesocellular carbon foam as a cathode and obtained higher capacity compared with several commercial black carbons [13]. Li et al. have reported that the graphene nanowalls have the capacity of 8705.9 mAh g^{-1}, and the capacity value is higher than those of carbon-based materials for the Li-O_2 battery [14]. Ouyang et al. have grown graphene directly on Ni foam via plasma-enhanced chemical vapor deposition (PECVD) at 950 ℃ and then anchored the MoS_2 nanowalls by using the hydrothermal method for the Li-ion battery [15]. They have observed that the addition of binders, like polyvinylidene difluoride and polytetrafluoroethylene, cause serious side reactions and capacity value decay [16]. Hu et al. have reported the binder-free N-doped holey-graphene for Li-O_2 batteries [17].

By contrast, noble metal nanoparticles (Pt, Ru, Pd, and Au) and metal oxides (MnO, Co_3O_4, and RuO_2) are extensively considered in combination with carbon materials for Li-O_2 batteries [8, 18]. These materials provide active sites and help tune the electrochemical activity. Many metal/metal oxide nanoparticles are used for Li-O_2 batteries. Among them, ruthenium nanoparticles (Ru NPs) are one of the most studied candidates for numerous applications because of their high catalytic activity toward the oxygen reduction/evolution reaction (ORR/OER) and excellent electrochemical stability. Jeong et al. have studied Pt, Pd, and Ru coatings for reducing graphene oxide for Li-O_2 batteries and claimed that the precious metals are capable of improving the OER efficiency [19]. Fan et al. have reported the transition metal carbide supported with VA-G by hot-filament chemical vapor deposition at high temperature as a superior catalyst for oxygen reactions [20]. Use of redox mediators to narrow down the overpotential of oxygen reactions in Li-O_2 batteries have been proven to be a viable option to enhance the stability of the cell [21]. Ghosh et al. have reported VA-G grown by PECVD with a variation of deposition parameters and examined it as potential anode material for Li-ion batteries [22]. In 2016, Su et al. have reported the ruthenium nanocrystal decorated VA-G to improve the stability of Li-O_2 batteries [23].

Here in the present report, we have grown VA-G on NF at room temperature. As a contrast to the reported growth techniques, our deposition of VA-G use conditions of low temperature with good control over the defects. We have systematically varied the deposition parameters like power, time and gas flow to obtain nanowalls of graphene aligning perpendicular to the substrate. This approach makes the present report unique from the reported articles. The as-prepared graphene films work as a binder-free cathode for Li-O_2 battery. Ru NPs were drop-casted on VA-G/NF to reduce the overpotential. We have successfully decreased the charge-overpotential and the charge-transfer resistance of the battery. Scheme 1 illustrates the process flow of PECVD and Ru NPs/VA-G/NF composite formation and cell configuration of the Li-O_2 battery.

2. Experimental section

2.1 Deposition of vertically-aligned graphene nanowalls on Nickel foam (VA-G/NF).

Deposition of VA-G/NF on pre-pressed nickel foam (NF) as a substrate with a diameter of 1.3 cm was carried out using commercial PECVD system (OPTHOS). The pre-deposition conditions e.g. cleaning of nickel foam and the deposition chamber was followed as per standard operating procedure. In details, the NF was cleaned ultrasonically in Acetone (Sigma-Aldrich, 99.5%) and 2-propanol (J.T.Baker) sequentially each for 3 minutes. Then, the cleaned substrates were dried under 3N N_2 gas flow. The deposition chamber was under running vacuum maintained at a base pressure of 0.02 Torr. The NF substrates were placed on a quartz holder and kept inside a quartz tube with diameter is 19 mm. Prior to the deposition,

the tube was cleaned by oxygen plasma created by the flow of oxygen at 40 sccm. All the depositions were carried out keeping the substrate at room temperature. The variables in the deposition process are microwave power, deposition time, the flow of reacting gas CH_4. The deposition conditions were varied one by one systematically keeping other parameters constant. For example, a constant flow of hydrogen as a carrier gas was maintained in the deposition chamber when we change the CH_4 flow. The deposition pressure was kept constant at 0.5 Torr in all the experiments. After the deposition, black coatings were observed on the substrate which was taken for further measurements.

2.2 Synthesis of ruthenium nanoparticles (Ru NPs).

The Ru NPs were synthesized by solvent reflux method, following the previously reported method [24]. In brief, the ruthenium chloride ($RuCl_3$ x H_2O: 49.6 mg) power first dissolved in 100 mL of ethylene glycol solution and the mixed solution were kept in an ultrasonic bath for 5 min. Afterward, the aforementioned sample was refluxed for 3 h at 170°C. After refluxing, the sample was cooled down to room temperature. Finally, the precipitation was filtered with deionized water and ethanol several times. The final product was dried in a vacuum oven at 70°C for 12 h.

2.3 Drop-casting ruthenium nanoparticles on VA-G/NF (Ru NPs/VA-G/NF)

The as-prepared Ru NPs were dispersed in 1-Methyl-2-pyrrolidone (NMP) (MACRON, >99.0%) solution (5 mg/ml) and 2 drops (10 µL pipet) were dropped on the VA-G/NF substrate. The loading weight was 4 mg. Subsequently, the substrate was dried overnight in a vacuum oven at 70°C and transferred into the glove-box for the Li-O_2 battery assembly.

2.4 Li-O_2 battery Coin cell assembly

The coin-type cell was assembled to examine the catalyst for possible application in Li-O_2 batteries. The coin-type battery has provision to close on one side where a Li-foil was placed, and the other side opened for exposure to oxygen gas from a cylinder. The Li-foil (0.5 mm thick), a glass fiber filter (GFF) separator, and an air electrode were squeezed inside of the coin-type battery. The GFF separator was soaked in the electrolyte, 1 M Bis(trifluoromethane)sulfonimide lithium salt (LiTFSI) (Sigma-Aldrich)/tetravinyl alcohol-dimethyl ether (TEGDME) (Sigma-Aldrich). The catalyst layer of the oxygen electrode was exposed to the electrolyte. The coin-cell was fixed in a specially designed glass bottle for electrochemical studies.

2.5 Characterization

Scanning electron microscopy (SEM, Hitachi S-4800, Japan) was used to characterize the morphology of the carbon materials at an acceleration voltage of 15.0 kV. The graphene nanowalls are characterized by high-resolution transmission electron microscopy (FE-HRTEM-EDX, JEOL-2100F). X-ray absorption spectroscopy (XAS) experiments were conducted at the 20A1 beamlines of the National Synchrotron Radiation Research Center (NSRRC) in Hsinchu city, Taiwan. Raman (DXR microscope, Thermo) spectrometers equipped with a 532 nm laser were used to obtain the Raman spectra of graphene film on nickel foam. Electrochemical impedance spectra (EIS) were recorded in a frequency of 1MHz to 0.1 Hz at an AC perturbation of 5 mV.

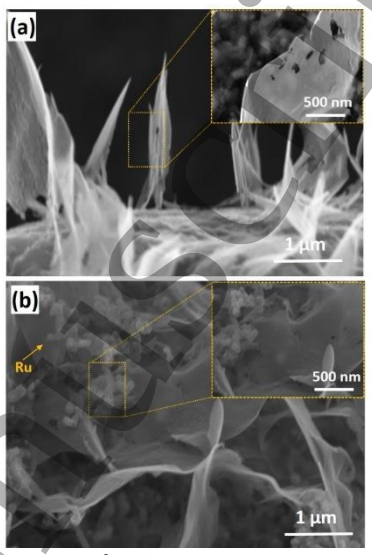

Figure 1. SEM of (a) As-grown VA-G/NF aligning perpendicularly to the NF surface (b) Drop-casted Ru NPs/VA-G/NF; showing agglomeration of Ru NPs. Insets present a magnified view of pristine and modified VA-G/NF. The deposition conditions; 60W, 5 min, 25 sccm H_2 and 2.0 sccm CH_4.

3. Results and discussion

The scanning electron microscopy (SEM) images of VA-G/NF and Ru NPs/VA-G/NF are shown in Figure 1. As shown in Figure 1(a)**,** the graphene nanowalls obtained on the Ni foam substrate via PECVD are grown perpendicularly to the substrate plane. In presence of the Ru NPs, agglomeration can be visible within the free space of graphene nanowalls, Figure 1(b). Insets of Figure 1 shows the high magnification SEM images, revealing holes on the surface of the graphene nanowalls. Presence of such holey structures on graphene sheets offers larger areas for the formation of Li_2O_2 during oxygen reactions [25]. Furthermore, the VA-G can provide a large area to accumulate the discharge products. Due to such a unique conformal coverage of Ru NPs on VA-G can boost the catalysis for oxygen reactions.

The corresponding high-resolution transmission electron microscopy (HRTEM) images of VA-G/NF and Ru NPs/VA-G/NF are shown in Figures 2(a) and **(**b). Transparent graphene sheets without Ru NPs shows occasional crumpling in Figure

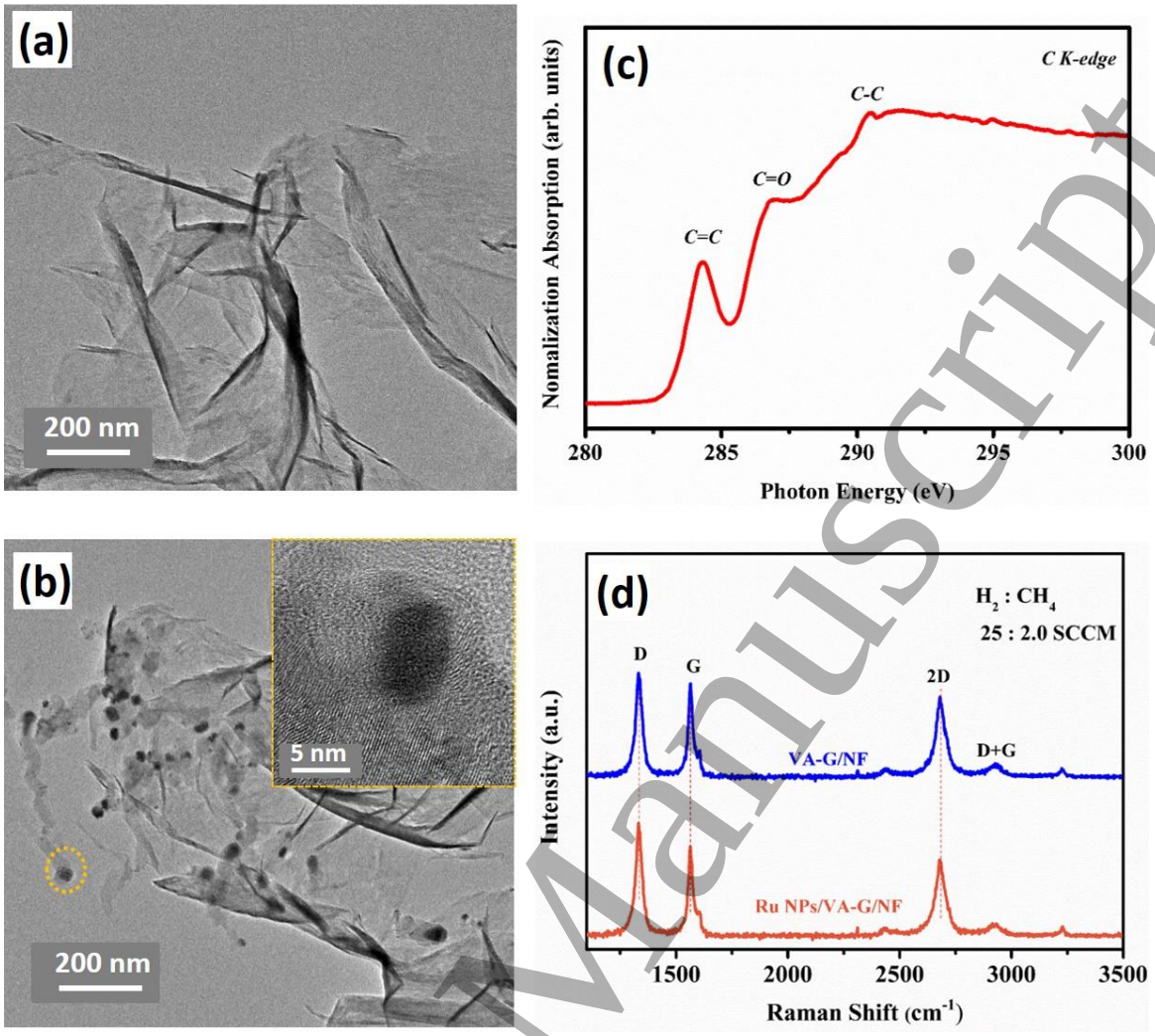

Figure 2. HRTEM images of the (a) VA-G/NF. (b) Ru NPs/VA-G/NF. composite materials. (c) C K-edge XANES spectra of VA-G/NF sample. (d) Raman spectra of the Ru NPs/VA-G/NF and VA-G/NF composite materials.

2(a). A uniform distribution of Ru NPs is clearly observed on the graphene surface Figure 2(b). The HRTEM image in the inset of indicates the Ru NPs are firmly embedded within the graphene sheets. Thickness contrast in both the images with and without Ru NPs may be an indication of the out of the plane growth of graphene sheets. Such a contrast has been observed in vertically grown edge rich graphene nanosheets [26]. The vertically aligned graphene sheets have several potential applications [27]. Figure 2(c) shows the X-ray absorption near edge structure (XANES) of C K-edge of the VA-G/NF sample. Three distinct peaks at 285.3, 289, and 292.2 eV can be attributed respectively to the C=C π^* excitation, C=O surface defects, and C–C σ^* excitation, in graphene [28, 29]. The XANES results are further compared with Raman spectra of the films. The conditions of PECVD are optimized to obtain VA-G nanowalls and characterized by Raman spectra, which provides information about the graphitization of different samples Figure 2(d) and Figure 3. Peaks in the Raman spectra are purely from the VA-G without any external additives. The bands at 1567.9 cm^{-1} are ascribed to the G band because of the E_{2g} vibrational modes of sp^2 carbon, whereas the band at 1334.5 cm^{-1} can be attributed to the D band because of the A_{1g} mode of sp^3 graphitic carbon materials. In addition, the 2D peak at 2679 cm^{-1} is due to the scattering of phonons by second-order vibration modes [30]. The multi-layer graphene is observed in the Raman spectra. The G to 2D band intensity ratio ~1. The G band from the in-planer vibration and the 2D band from double resonance scattering [31]. SEM and TEM images reveal the PECVD grown VA-G/NF are multi-layered. Use of metallic substrates like NF is essential for growth of graphene as they are capable of decomposing hydrocarbons like CH_4 and can promote the nucleation for graphene [32].

During the PECVD growth process, a steady flow rate of methane gas (CH_4) is supplied in the growth chamber, which is decomposed by hydrogen plasma and the resulting carbon atoms are deposited onto the NF substrate and resulted in vertically aligned graphene nanowalls on the NF substrate [33]. The direct growth of graphene on NF surface has the

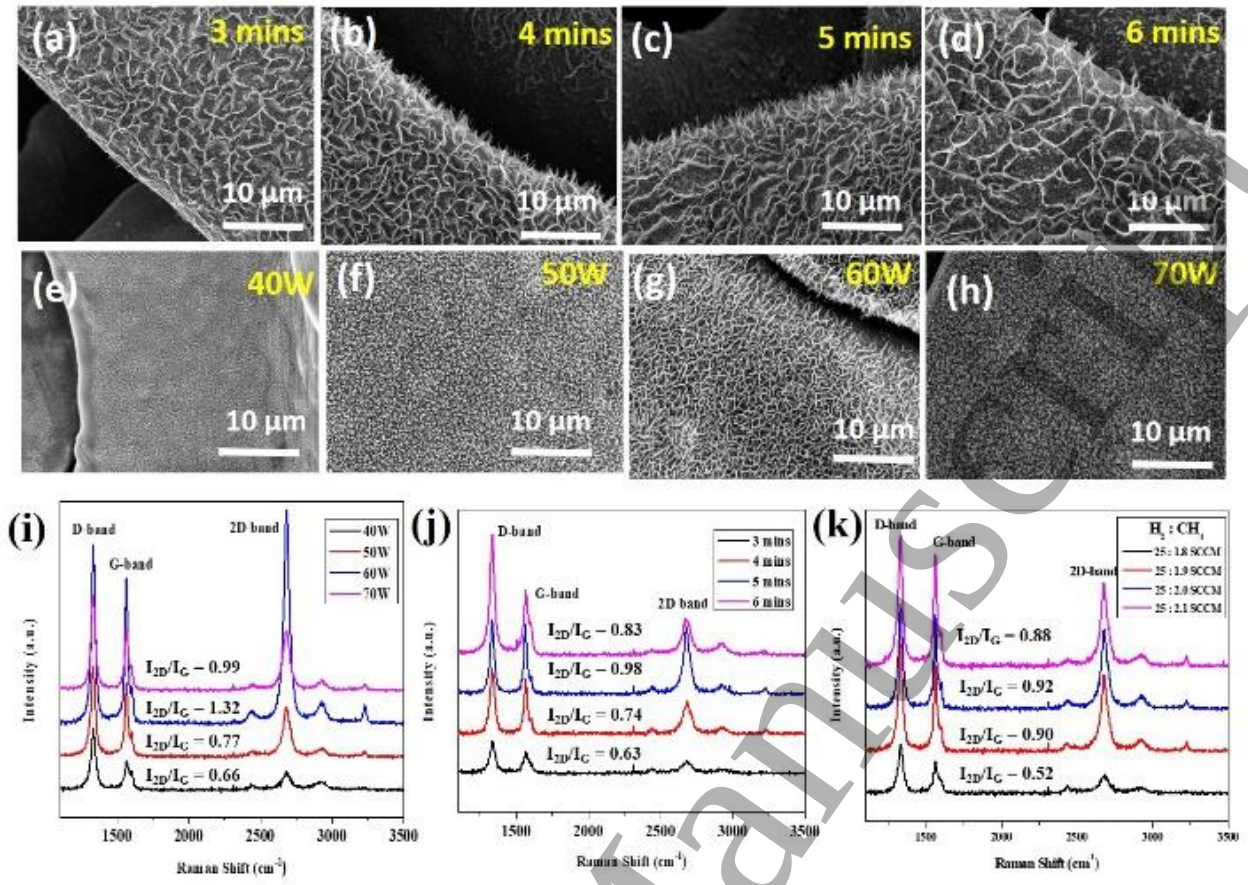

Figure 3. (a-d) SEM images of VA-G/NF with variation in deposition time from 3 to 6 min at a constant power of 60W and CH_4 flow of 2.0 sccm, (e-h) SEM images of VA-G/NF materials with change in microwave power from 40 to 70 W keeping the flow rate of CH_4 and deposition time constant at 2.0 sccm and 5 min. respectively. Raman spectra of the VA-G/NF (i) with change in microwave power keeping the flow rate of CH_4 and deposition time constant at 2.0 sccm and 5 min. respectively, (j) with variation in deposition time keeping power constant at 60W and flow of CH_4 constant at 2.0 sccm, and (k) with change in flow rates of CH_4 keeping power constant at 60W and deposition time 5 min.

advantage of achieving binder-free composite materials as the cathode for Li-O_2 batteries. The defect intensity ratios (I_D/I_G) of the Ru NPs/VA-G/NF and VA-G/NF composite materials are 0.92 and 0.85, respectively (optimum conditions = H_2 : 25; CH_4 : 2.0 sccm). Moreover, we selected different methane flow rates to analyze the surface changes. We found that robust graphene walls could be achieved at 2.0 sccm (CH_4). The amount of methane could affect the deposition of graphene. Since deriving an absolute mechanism for the growth of graphene by PECVD is cumbersome, within the boundary of allowable parameter variations in the current PECVD instrument, we have tried to get the optimized conditions to grow the VA-G nanowalls. Jones et al. have presented the control over the graphene layers with hydrogenation [34]. The residual gas analyzer pattern is shown in figure S1. Furthermore, with the addition of Ru NPs on the graphene surface, the D and G band intensity doesn't show any change in figure 2(d), We have extended the study with varying the deposition parameters further, such as power, deposition time, and H_2 flow rate.

To understand the effect of growth time, we have varied the deposition time with the constant power of 60W and 2.0 sccm flow of CH_4. As shown in the SEM images in Figure 3(a) to (d), with increase in deposition time, the edge sites of NF substrates are coated with VA-G till 5 min deposition time. However, the density of the VA-G on the edges of NF decreases at 6 min deposition time in Figure 3(d). Our experimental results show that five-minute deposition time yielded a high-intensity 2D band, as manifested by the Raman spectra in Figure 3(j). With the increasing deposition time, no peak shift is observed, whereas the D band peak intensified. Additionally, we investigated the effects of varying flow rates of CH_4, and the resulting Raman spectra of samples growth under different flow rates are shown in Figure 3(k). The result suggested that the 2.0 sccm flow rate appear to be the best

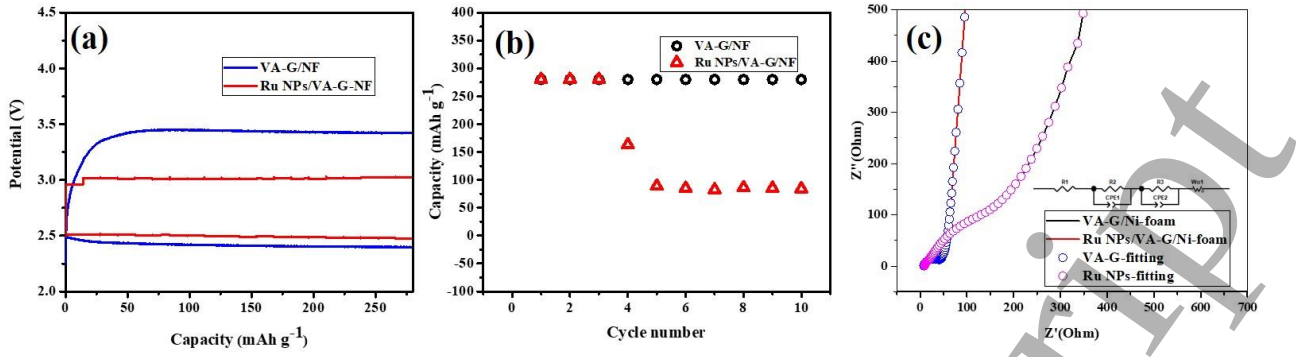

Figure 4. (a) Discharge/charge voltage profiles. (b) Variation of discharge capacity with cycle number of the Ru NPs/VA-G/NF and (c) Nyquist plots of Ru NPs/VA-G/NF and VA-G/NF electrode (The experience condition was under 60W, 5 min, 25 sccm H_2, and 2.0 sccm CH_4).

condition due to the ratio of G and 2D band have the much higher value near 1. Based on the Raman spectroscopic studies, we conjecture that the aforementioned PECVD growth conditions favor multi-layer graphene growth. The PECVD grew Ru NPs/VA-G/NF and VA-G/NF samples are further characterized by electrochemical techniques for their viability as an electrode in Li-O_2 batteries.

As reported earlier, the microwave power has a significant effect on the quality of graphene, we have varied the microwave power from 40 W to 70 W to optimize the graphene growth keeping the flow rate of CH_4 and deposition time constant at 2.0 sccm and 5 min. respectively [35]. At 40W microwave power, insufficient decomposition of CH_4 renders in inadequate films. With increasing microwave power, the growth rate of graphene improved, and optimized graphene growth achieve at 60 W as shown in SEM images in Figures 3(e)-3(h). Further increase of the microwave power resulted in the lower growth rate of graphene nanowalls due to plasma-induced damage. The corresponding Raman spectra are shown in Figure 3(i). We can observe near 2D-band there have some peaks. We believe it is a satellite peak for 2D-band[36]. From these studies, we conclude that 60 W microwave power is the optimum condition for further studies because of the ratio about G and 2D band near 1.

A set of discharge/charge and cycles performance is recorded. The first cycle discharge/charge voltage profile of Ru NPs/VA-G/NF and VA-G/NF electrodes at 140 mAg^{-1} current density is shown in Figure 4(a). Here, the VA-G/NF sample are grown by using power 60W, 5 min, 25 H_2 sccm and CH_4 2.0 sccm. We utilized the sample for the further use because it has higher 2D to G band observed in the Raman spectra. The ratio higher than 1 or near 2, the graphene more like double-layer or a single layer. Su et al. have used Ru/VA-G/NF with 50 cycles using higher microwave 1000 W power and 400 ℃ substrate temperature [23]. In addition, they have used solution methods to add Ru. In the current report, the charge overpotential reduces below 0.5 V in the Ru/VA-G/NF sample. The overpotential is smaller than the VA-G/NF electrode. The charging and discharging plateaus are approximately 3.0 and 2.5 V, respectively, for the Ru NPs/VA-G/NF electrode. This improved performance may be because Ru NPs provides active sites during the charge/discharge cycle, thus reducing the overpotential. The OER part is also dramatically reduced by the addition of Ru NPs because of the strong reaction of Ru to the Li_2O_2 discharge product and reduction. Furthermore, the cycle durability is an important factor of consideration for the Li-O_2 battery. Figures 4(b) show the variation of discharge capacity with cycle number for the Ru NPs/VA-G/NF and VA-G/NF electrodes at 140 mA g^{-1} current density. The pure VA-G/NF electrode shows the cycle number with discharge capacity 10 cycles. By contrast, the Ru NPs/VA-G/NF electrode exhibited satisfactory the cycle number with discharge capacity only has 10 cycles. Therefore, the electrode doesn't provide stable performance at discharge/charge cycles. We suspect the drop casting Ru NPs after view cycle will influence the Li_2O_2 storage, cause the capacity lower than the first cycle. The Nyquist plots of Ru NPs/VA-G/NF and VA-G/NF battery cells are shown in Figure 4(c). The R_1 and R_2 are the ohmic resistance of the electrolyte and the charge transfer resistance (CPE), respectively. In VA-G/NF, the values of R_1, R_2, and R_3 are 9.02, 9.33, and 5.22, respectively. Consequently, the R_1, R_2, and R_3 values of Ru NPs/VA-G/NF are 7.93, 6.06, and 27.42, respectively. The first semi-circle is corresponding to the interfacial resistance between graphene and NF, a second semi-circle is corresponding to the Ru NPs charge transferred to the electrolyte solution. Thus, the enhancement of electrical conductivity is due to the combination of conductive Ru NPs and VA-G [37]. In addition, the data is fitted and the resultant equivalent circuit model presented inset in Figure 4(c). Continuous deposition of lower conducting Li_2O_2 on the surface increases the cell impedance, and obstructs the electron transfer and hence rise in overpotential [38, 39]. The charge-discharge overpotential makes us realize the electric charger transfer between VA-G and Ru NPs in Li-O_2 battery.

4. Conclusions

In summary, we have successfully developed VA-G/NF electrodes by means of room temperature PECVD method. By further drop-casting Ru NPs onto the VA-G/NF substrate, we have demonstrated binder-free Ru NP/VA-G/NF electrodes for Li-O_2 battery. The charging overpotential is found to decrease from 3.5 V to 3.0 V after the incorporation of Ru NPs into the VA-G/NF substrate. The VA-G/NF samples offered fast electron transfer from the Ni foam to the surface graphene and also reacted with oxygen in the Li-O_2 battery. This work, therefore, offers a new approach to synthesizing graphene electrodes for Li-O_2 and Li-CO_2 batteries.

Acknowledgments

We thank the financial support from the Ministry of Science and Technology (Contract Nos. MOST 106-2112-M-003-007-MY3 and MOST 107-2113-M-002-008-MY3).

References

[1] Liu Y, Wang L, Cao L, Shang C, Wang Z, Wang H, He L, Yang J, Cheng H, Li J and Lu Z 2017 Understanding and Suppressing Side Reactions in Li-Air batteries *Mater. Chem. Front.* **1** 2495−510

[2] Chang Z, Xu J and Zhang X 2017 Recent Progress in Electrocatalyst for Li-O_2 Batteries *Adv. Energy Mater*. **7** 1700875

[3] Luntz A C and McCloskey B D 2014 Nonaqueous Li–Air Batteries: A Status Report *Chem. Rev.* **114** 11721−50

[4] Chen W, Gong Y F and Liu J H 2017 Recent Advances in Electrocatalysts for Non-Aqueous Li–O_2 Batteries *Chin. Chem. Lett.* **28** 709−18

[5] Bruce P G, Freunberger S A, Hardwick L J and Tarascon J M 2011 Li–O_2 and Li–S Batteries with High Energy Storage *Nat. Mater.* **11** 19−29

[6] Yoon K R, Lee G Y, Jung J W, Kim N H, Kim S O and Kim I D 2016 One-Dimensional RuO_2/Mn_2O_3 Hollow Architectures as Efficient Bifunctional Catalysts for Lithium–Oxygen Batteries *Nano Lett.* **16** 2076−83

[7] Aurbach D, McCloskey B D, Nazar L F and Bruce P G 2016 Advances in Understanding Mechanisms Underpinning Lithium–Air Batteries *Nat. Energy* **1** 16128

[8] Tan P, Wei Z H, Shyy W, Zhao T S and Zhu X B 2016 A Nano-Structured RuO_2/NiO Cathode Enables the Operation of Non-Aqueous Lithium-Air Batteries in Ambient Air *Energy Environ. Sci.* **9** 1783−93

[9] Wang G, Huang L, Huang W, Xie J, Du G, Zhang S, Zhu P, Cao G and Zhao X 2015 Nanostructured Porous RuO_2/MnO_2 as a Highly Efficient Catalyst for High-Rate Li-O_2 Batteries *Nanoscale* **7** 20614−24

[10] Abraham K M and Jiang Z 1996 A Polymer Electrolyte-Based Rechargeable Lithium/Oxygen Battery *J. Electrochem. Soc.* **143** 1−5

[11] Boyd D A, Lin W H, Hsu C C, Teague M L, Chen C C, Lo Y Y, Chan W Y, Su W B, Cheng T C, Chang C S, Wu C I and Yeh N C 2015 Single-step deposition of high-mobility graphene at reduced temperatures *Nat. Commun.* **6** 6620

[12] Hsu C C, Bagley J D, Teague M L, Tseng W S, Yang K L, Zhang Y, Li Y, Li Y, Tour J M and Yeh N C 2018 High-Yield Single-Step Catalytic Growth of Graphene Nanostripes by Plasma Enhanced Chemical Vapor Deposition *Carbon* **129** 527−36

[13] Yang X H, He P and Xia Y Y 2009 Preparation of Mesocellular Carbon Foam and Its Application for Lithium/Oxygen Battery *Electrochem. Commun.* **11** 1127−30

[14] Li Y, Wang J, Li X, Geng D, Li R and Sun X 2011 Superior Energy Capacity of Graphene Nanosheets for a Nonaqueous Lithium-Oxygen Battery *ChemComm* **47** 9438−40

[15] Ouyang B, Wang Y, Zhang Z and Rawat R S 2016 MoS_2 Anchored Free-Standing Three Dimensional Vertical Graphene Foam Based Binder-Free Electrodes for Enhanced Lithium-Ion Storage *Electrochim. Acta* **194** 151−60

[16] Riaz A, Jung K N, Chang W, Shin K H and Lee J W 2014 Carbon-, Binder-, and Precious Metal-Free Cathodes for Non-Aqueous Lithium–Oxygen Batteries: Nanoflake-Decorated Nanoneedle Oxide Arrays *ACS Appl. Mater. Interfaces* **6** 17815−22

[17] Shui J, Lin Y, Connell J W, Xu J, Fan X and Dai L 2016 Nitrogen-Doped Holey Graphene for High-Performance Rechargeable Li–O_2 Batteries *ACS Energy Lett.* **1** 260−5

[18] Ma S, Wu Y, Wang J, Zhang Y, Zhang Y, Yan X, Wei Y, Liu P, Wang J, Jiang K, Fan S, Xu Y and Peng Z 2015 Reversibility of Noble Metal-Catalyzed Aprotic Li-O_2 Batteries *Nano Lett.* **15** 8084-90

[19] Jeong Y S, Park J B, Jung H G, Kim J, Luo X, Lu J, Curtiss L, Amine K, Sun Y K, Scrosati B and Lee Y J 2015 Study on the Catalytic Activity of Noble Metal Nanoparticles on Reduced Graphene Oxide for Oxygen Evolution Reactions in Lithium–Air Batteries *Nano Lett.* **15** 4261−8

[20] Fan X, Peng Z, Ye R, Zhou H and Guo X 2015 M_3C (M: Fe, Co, Ni) Nanocrystals Encased in Graphene Nanoribbons: An Active and Stable Bifunctional Electrocatalyst for Oxygen Reduction and Hydrogen Evolution Reactions *ACS Nano* **9** 7407−18

[21] Zhang J, Sun B, Zhao Y, Kretschmer K and Wang G 2017 Modified Tetrathiafulvalene as an Organic Conductor for Improving Performances of Li−O_2 Batteries *Angew. Chem. Int. Ed.* **56** 8505−9

[22] Ghosh M, Venkatesh G and Rao G M 2016 Surface Modification of Vertically Aligned Graphene Nanosheets by Microwave Assisted Etching for Application as Anode of Lithium Ion Battery *Solid State Ion.* **296** 31−6

[23] Su D, Han Seo D, Ju Y, Han Z, Ostrikov K, Dou S, Ahn H J, Peng Z and Wang G 2016 Ruthenium Nanocrystal Decorated Vertical Graphene Nanosheets@Ni Foam as Highly Efficient Cathode Catalysts for Lithium-Oxygen Batteries *NPG Asia Mater*. **8** e286

[24] Yang S, Qiao Y, He P, Liu Y, Cheng Z, Zhu J J and Zhou H 2017 A Reversible Lithium-CO_2 Battery with Ru Nanoparticles as a Cathode Catalyst *Energy Environ. Sci.* **10** 97−978

[25] Lin Y, Moitoso B, Martinez-Martinez C, Walsh E D, Lacey S D, Kim J W, Dai L, Hu L and Connell J W 2017 Ultrahigh-Capacity Lithium–Oxygen Batteries Enabled by Dry-Pressed Holey Graphene Air Cathodes *Nano Lett.* **17** 3252−60

[26] Song Q, Yan H, Liu K, Xie K, Li W, Gai W, Chen G, Li H, Shen C, Fu Q, Zhang S, Zhang L and Wei B 2018 Vertically Grown Edge-Rich Graphene Nanosheets for Spatial Control of Li Nucleation *Adv. Energy Mater.* **8** 1800564

[27] Han Z J, Pineda S, Murdock A T, Seo D H, Ostrikov K and Bendavid A 2017 RuO_2-Coated Vertical Graphene Hybrid Electrodes for High-Performance Solid-State Supercapacitors *J. Mater. Chem. A* **5** 17293-301

[28] Geng D, Yang S, Zhang Y, Yang J, Liu J, Li R, Sham T K, Sun X, Ye S and Knights S 2011 Nitrogen Doping Effects on the Structure of Graphene *Appl. Surf. Sci.* **257** 9193−8

[29] Zhong J, Deng J J, Mao B H, Xie T, Sun X H, Mou Z G, Hong C H, Yang P and Wang S D 2012 Probing Solid State N-Doping in Graphene by X-Ray Absorption Near-Edge Structure Spectroscopy *Carbon* **50** 335−8

[30] Niyogi S, Bekyarova E, Itkis M E, Zhang H, Shepperd K, Hicks J, Sprinkle M, Berger C, Lau C N, deHeer W A, Conrad E H and Haddon R C 2010 Spectroscopy of Covalently Functionalized Graphene *Nano Lett.* **10** 4061−6

[31] Das A, Chakraborty B and Sood A K 2008 Raman Spectroscopy of Graphene on Different Substrates and Influence of Defects *Bull. Mater. Sci.* **31** 579-84

[32] Kato T and Hatakeyama R 2012 Direct Growth of Doping-Density-Controlled Hexagonal Graphene on SiO_2 Substrate by Rapid-Heating Plasma CVD *ACS Nano* **6** 8508-15

[33] Reina A, Jia X, Ho J, Nezich D, Son H, Bulovic V, Dresselhaus M S and Kong J 2009 Large Area, Few-Layer Graphene Films on Arbitrary Substrates by Chemical Vapor Deposition *Nano Lett.* **9** 30−5

[34] Jones J D, Hoffmann W D, Jesseph A V, Morris C J, Verbeck G F and Perez J M 2010 On the Mechanism for Plasma Hydrogenation of Graphene *Appl. Phys. Lett.* **97** 233104

[35] Herrebout D, Bogaerts A, Yan M, Gijbels R, Goedheer W and Dekempeneer E 2001 One-Dimensional Fluid Model for an Rf Methane Plasma of Interest in Deposition of Diamond-Like Carbon Layers *J. Appl. Phys.* **90** 570-9

[36] Castriota M, Cazzanelli E, Pacilè D, Papagno L, Girit Ç O, Meyer J C, Zettl A, Giarola M and Mariotto G 2010 Spatial dependence of Raman frequencies in ordered and disordered monolayer graphene *Diamond Relat. Mater.* **19** 608-13

[37] Li F, Tang D M, Jian Z, Liu D, Golberg D, Yamada A and Zhou H 2014 Li-O_2 Battery Based on Highly Efficient Sb-Doped Tin Oxide Supported Ru Nanoparticles *Adv. Mater.* **26** 4659−64

[38] Zeng X, You C, Leng L, Dang D, Qiao X, Li X, Li Y, Liao S and Adzic R R 2015 Ruthenium Nanoparticles Mounted on Multielement Co-Doped Graphene: An Ultra-High-Efficiency Cathode Catalyst for Li-O_2 Batteries *J. Mater. Chem. A* **3** 11224–31

[39] Xia C, Waletzko M, Chen L, Peppler K, Klar P J and Janek J 2014 Evolution of Li_2O_2 Growth and Its Effect on Kinetics of Li–O_2 Batteries *ACS Appl. Mater. Interfaces* **6** 12083−92